Published March 14, 2019

Technical Notes

Core Ideas

- Long-term irrigation with brackish water can extend the practice into water-scarce regions.
- ESEM in both dynamic and static modes is a promising technique to analyze soil impacts.
- Changes linked to the hydrophilic behavior of soils can be detected.

Environmental Scanning Electron Microscopy Application for Brackish Water Irrigation Impact on Soil

J. Valdes-Abellan,* L. Candela, G. M. Medero, and J. Buckman

We investigated soil response to irrigation with slightly brackish water (1200 mg L^{-1} total dissolved solids on average) in a semiarid environment at the microscopic scale using environmental scanning electron microscopy (ESEM) applied in static and dynamic modes, which allowed comparison between nonirrigated and 3-yr-irrigated soil samples to determine the impact of applied brackish water. Results indicate that (i) there was a change in soil hydrophilic behavior by the continuous accumulation of water-borne salt in the soil matrix, (ii) compared with nonirrigated samples, the wetting process occurred more gradually for the 3-yr-irrigated sample, (iii) the wetting process started at a lower vapor pressure for the 3-yr-irrigated sample, (iv) water vapor pressure in the chamber at full saturation was lower for the 3-yr-irrigated sample, and (v) the presence of heavy metals in the soil was more frequent in irrigated samples. Our results show that ESEM is a useful technique to determine the impacts on soil of irrigation with slightly brackish water.

Abbreviations: EDX, energy dispersive X-ray; ESEM, environmental scanning electron microscopy; RH, relative humidity.

The use of unconventional water (e.g., desalted or treated wastewater) for irrigation is becoming common in water-scarce regions of the world (Ghermandi and Messalem, 2009; Martínez Beltrán and Koo-Oshima, 2004). Among the different types of unconventional water, desalted water mixed with raw saline water is a common agricultural strategy in water-scarce areas (Valdes-Abellan et al., 2013). This mixing provides brackish water that can be applied to the field.

Soil column experiments to assess the impacts of irrigation with unconventional water have been conducted more frequently with treated wastewater (Assouline and Narkis, 2011, 2013) than with salted water (Beltrán, 1999; Lado and Ben-Hur, 2010). Research has mainly focused on saturated hydraulic conductivity change (Dikinya et al., 2008; Mandal et al., 2008) by pore clogging, dissolved organic matter, or clay dispersion (Lado and Ben-Hur, 2009). Saturated hydraulic conductivity has been usually obtained in the laboratory with constant-head permeability tests or by single- or double-ring infiltrometers (Dane and Topp, 2002) in the field.

Environmental scanning electron microscopy (ESEM) requires minimal sample preparation for analyzing microscopic changes in soil structure and soil wetting patterns (Farulla et al., 2010; Koliji et al., 2010; Lourenço et al., 2008). A number of ESEM applications to explore fundamental properties of water retention characteristics, permeability, and micro- and macrostructural interactions in geologic materials have been reported by Romero and Simms (2008). Using ESEM, Donald (1998) investigated wet systems and the important role of soil water content in water flow and contaminant processes, and Ali and Barrufet (1995) studied porous media. However, to our knowledge, the influence of brackish water application on soil wettability patterns due to long-term irrigation has received less attention.

The main objective of this research is the microscale assessment of wetting and drying patterns from vadose zone soil samples by ESEM and a comparison with in situ results. Soil samples were collected before and after 3 yr of irrigation with brackish water from a

J. Valdes-Abellan, Dep. of Civil Engineering, Univ. of Alicante, Alicante, Spain; L. Candela, Dep. of Civil and Environmental Engineering, Univ. Politècnica de Catalunya, 08034 Barcelona, Spain; G.M. Medero, Institute for Infrastructure & Environment, School of Energy, Geoscience, Infrastructure and Society, Heriot-Watt Univ., Edinburgh, Scotland EH14 4AS, UK; J. Buckman, Institute of Petroleum Engineering, Heriot-Watt Univ., Edinburgh, Scotland EH14 4AS, UK. *Corresponding author (javier.valdes@ua.es).

Received 12 Mar. 2018.
Accepted 14 Nov. 2018.

Citation: Valdes-Abellan, J., L. Candela, G.M. Medero, and J. Buckman. 2019. Environmental scanning electron microscopy application for brackish water irrigation impact on soil. Vadose Zone J. 18:180046. doi:10.2136/vzj2018.03.0046

monitored experimental plot located in a semiarid area (Alicante, southeastern Spain).

Material and Methods

Study Site and Field Experiment

Soil samples were obtained from an experimental plot (9 by 5 m) with no previous agricultural practices at the University of Alicante in southeastern Spain. After turfgrass plantation, irrigation with brackish water started in July 2011 and continued until 2018; the amount of irrigation followed plant demand. The climate is semi-arid, with an average annual rainfall rate of 330 mm and average annual potential reference evapotranspiration of 1200 mm following the Penman–Monteith method (Allen et al., 1998).

Disturbed and undisturbed soil samples (collected with 5-cm o.d. steel rings) were obtained for laboratory characterization. Soil bulk density (Grossman and Reinsch, 2002), particle size distribution (Gee and Or, 2002), porosity (Flint and Flint, 2002b), and soil particle density (Flint and Flint, 2002a) were determined. Samples for ESEM were collected at 40 cm depth in June 2011, before the beginning of the irrigation period. The second set of samples were obtained in June 2014 after 3 yr of continuous irrigation at the same depth. The 40-cm depth assured the absence of root activity and the avoidance of other factors that affect hydrophilicity, such as the production of organic matter by roots. The soil water model has been described (Valdes-Abellan et al., 2015). Conservative solute transport was previously done, and results are presented in Valdes-Abellan et al. (2014).

Irrigation Water Quality

The water applied for irrigation is a blend of raw brackish and desalted groundwater from a reverse-osmosis desalination plant (Prats and Chillón Arias, 2001; Prats et al., 1997). Major ion analysis in irrigation water took place monthly; in situ determination of pH, temperature (°C), potential redox (Eh), and electrical conductivity (μS cm^{-1}) was performed with an Eijkelkamp 18.28 Multiparameter Analyzer. Table 1 summarizes the hydrochemical information of interest.

Environmental Scanning Electron Microscopy Testing

Soil structure, mineralogy, and pore size distribution of the soil samples were investigated by ESEM, which allows the analysis of undisturbed samples under static or dynamic mode with regard to the relative humidity (RH) and temperature inside the chamber.

The apparatus (a Quanta 650 FEG SEM and an FEI XL30 LaB_6 ESEM) was equipped with large-area energy dispersive X-ray (EDX) detectors (X-Max, Oxford Instruments) for elemental analysis. The scanning electron microscope was operated in either low-vacuum or full ESEM wet mode. Water vapor was used to improve the image quality based on previous studies (Forster et al., 2008).

Samples used in the ESEM have irregular shapes due to the sampling process from field-site undisturbed soil samples (soil cores). The maximum size of the analyzed samples was ~0.9 to 1 cm, and the minimum size was 2 to 3 mm; all samples were of approximately lenticular shape and size. We assumed there was no temperature gradient inside the soil sample considering the small size and the large specific surface derived from the lentil shape.

Static Mode of Environmental Scanning Electron Microscopy

Two uncoated and undisturbed soil samples were imaged in low-vacuum mode (5°C and 10% RH or 0.7 mm Hg) at low magnification. Specific areas of interest were defined for higher-resolution analysis. The accelerating voltage was 20 kV. Microscope images were obtained from a gaseous secondary electron detector or a backscattered electron detector. The working distance was ~10 mm, and the spot size was 4.5 to 5.3 mm.

Carbon-coated polished blocks of samples were examined using the Quanta 650 FEG scanning electron microscope. This technique has the advantage of providing large-scale areas at high resolution, allowing the detection of changes in soil structure (Buckman, 2014). In addition, EDX analysis was applied in selected areas to determine mineral phase.

Dynamic Mode of Environmental Scanning Electron Microscopy

The dynamic mode of the ESEM lets water condense on, or sublimate from, the sample surface by controlling water vapor pressure and the temperature inside the chamber. A Peltier cooling stage controls the temperature to within 20°C; vapor pressure can be increased to 2.67 kPa (20 mm Hg). Thus, wetting–drying patterns and interactions between solid and liquid phases within the soil matrix can be obtained (Forster et al., 2008; Lourenço et al., 2008, 2012).

Table 1. Irrigation water physicochemical characteristics.

Parameter†	Jan.	Feb.	Mar.	Apr.	May	June	July	Aug.	Sept.	Oct.	Nov.	Dec.
pH	7.90	7.95	8.10	7.80	7.90	8.11	8.28	8.60	8.30	7.70	7.70	7.10
EC, μS cm^{-1}	2090	1755	1677	2070	2160	1822	1890	1277	1707	1809	1132	1134
Hardness, mg L^{-1} $CaCO_3$	396.5	327.3	303.9	368.6	434.7	398.0	352.2	347.9	427.6	343.9	314.1	225.5
Alk TAC, mg L^{-1} HCO_3	132.3	110.0	117.0	154.9	133.7	132.1	152.2	133.9	164.2	114.4	158.9	86.7
SAR	5.75	5.53	5.30	5.19	6.13	5.26	4.11	4.85	4.79	5.32	3.47	4.18

† EC, electrical conductivity; Alk TAC, alkalinity to pH 4.5; SAR, sodium adsorption ratio.

In the experiment, the temperature was maintained at 5°C, and RH was controlled by increasing the water vapor pressure from 5 to 6.5 mm Hg, giving 77 to 100% RH. Low chamber temperature allows saturation with low water vapor pressure. Accordingly, the quality of digital images obtained during the test increases because fewer particles exist in the pressure chamber and scattering from the electron beam is lower. Dynamic wetting and drying tests started at 77% RH (5 mm Hg water vapor pressure), and the rate steadily increased to achieve complete saturation of the sample; it was followed by a vapor pressure decrease to its initial value for obtaining the drying part of the cycle. The wetting–drying cycle was replicated three times with each sample.

Results and Discussion

From the analysis of the soil samples, two soil layers were defined (Table 2): (i) an upper layer of clayey loam (from the surface to 5–6-cm depth) where grass roots mainly develop and (ii) a second layer (up to ~40 cm) of sandy loam with significantly lower content of organic matter and with almost no roots present. Table 2 provides detailed information about the two layers. According to X-ray mineralogy, calcite was the most important mineral in both layers. Clay mineral content (illite) in Layer 1 accounted for up to 9.7% and was practically absent in Layer 2 (Table 2). Detailed site descriptions can be found in previous studies (Valdes-Abellan et al., 2015, 2017).

Table 2. Summary of soil physical properties and mineralogical content.

Parameter†	Layer 1	Layer 2
Depth, m	0–0.05	0.05–0.40
Sand–silt–clay, %	36.2–29.6–34.2	59.1–34.8–6.0
Texture	clay loam	sandy loam
Bulk density, g cm^{-3}	1.38	1.5
Porosity, %	47	41
Soil particle density, g cm^{-3}	2.65	2.53
X-ray mineralogy, %		
Calcite	67.2	81.4
Quartz	18.1	9.1
Gypsum	ND‡	6.9
Illite	9.7	2.1
Dolomite	5	0.6
CEC, cmol kg^{-1}	12.4	4.7
OM, % C of dry soil weight	0.8	0.21

† CEC, cation exchange capacity; OM, organic matter.
‡ Not detected.

Static Mode Results

The static ESEM mode shows an overall uniform sample composition of small calcite crystals covering the surface with some silica particles or calcite structures. Our study confirms the presence of Sr, which was previously recorded by Valdes-Abellan et al. (2014). Figure 1 presents information about a soil sample prior to irrigation at different scale resolution. Figure 1a shows a general view of the sample surface, with Ca as the prevalent mineral from EDX analysis. In Fig. 1b a silica grain is observed, and Fig. 1c shows a Ca tubular structure.

For the sample collected after 3-yr irrigation, results show that the main features of the nonirrigated sample remain; Ca was the

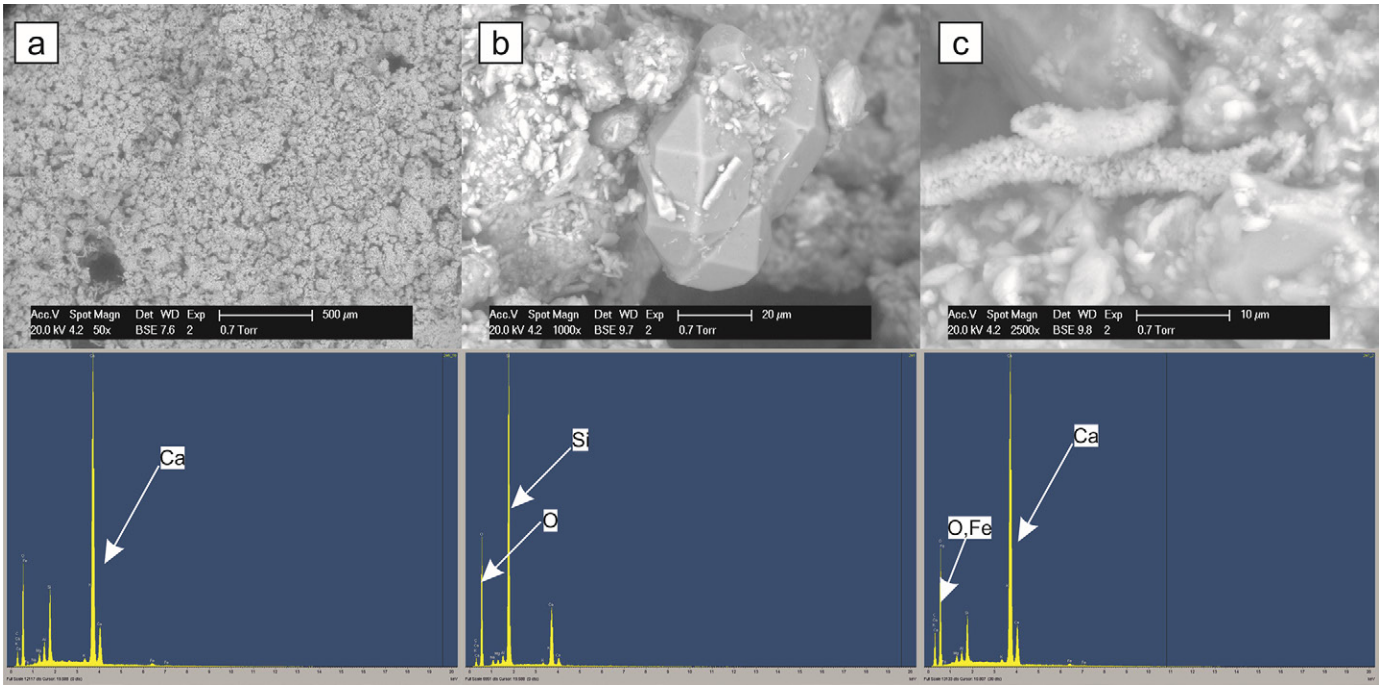

Fig. 1. Micrographs and energy dispersive X-ray analysis prior to irrigation for (a) a general view of the sample surface, (b) a silica grain, and (c) a Ca tubular structure.

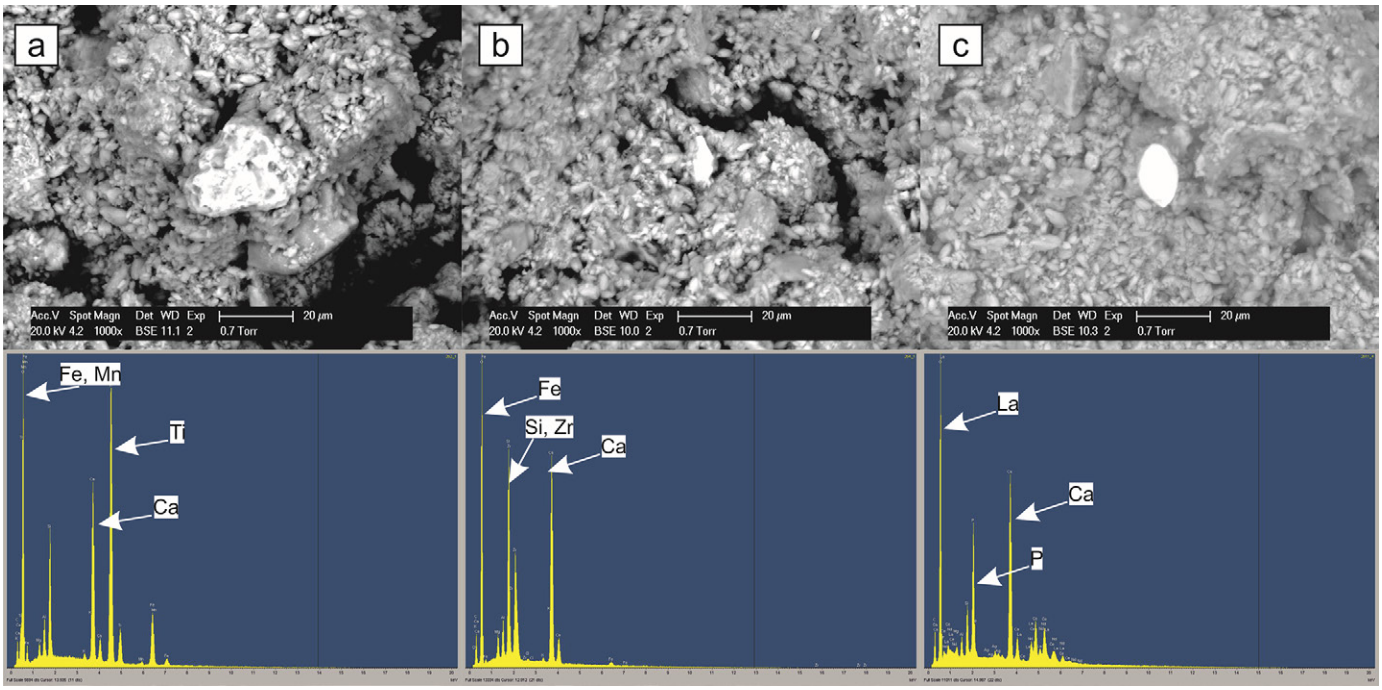

Fig. 2. Micrographs and energy dispersive X-ray analysis for different bright spots located in the 3-yr-irrigated sample: (a) Fe and Mn; (b) mainly Fe; and (c) La.

main element present followed by silica, with calcite and quartz being the prevalent minerals. The application of static mode let us identify two important facts: (i) the number of calcite tubular structures increases in irrigated samples, and (ii) the presence of heavy metals (e.g., Zr, Sr, and Fe) increases significantly.

The detection of existing heavy metals is relatively straightforward using backscattered electron images because the higher the molecular weight of the elements, the brighter than the surrounding matrix is the spot where those elements are located. An example of this feature can be seen in Fig. 2, where three bright spots were identified, and the application of EDX on these locations revealed the presence of titanium, zirconium, and/or lanthanum. The EDX analysis was applied in both specific locations and maps. Results from EDX mapping (Fig. 3) are in agreement with the abovementioned specific EDX analyses together with soil sample mineralogy and composition determined by X-ray fluorescence and diffractometric methods (Table 2).

Dynamic Mode

Figure 4 presents the wetting and drying paths in the nonirrigated soil sample. Calcite minerals and some silica particles are observed during the process. Once the RH reached 98.3 to 100%, the vapor pressure value reached 6.4 to 6.5 mm Hg, and the saturation process developed very rapidly. During the wetting path (Fig. 4a and 4b), water initially fills the smaller pores and later fills the macropores, and menisci formation due to water vapor pressure increase is observed. In Fig. 4c, the meniscus radius ranging from 3 to 6 μm is highlighted. Given a meniscus radius of 5 μm, the temperature in the chamber should be 4.8°C according to the Kelvin equation (Andraski and Scanlon, 2002), which agreed with the previously established temperature of 5°C. Temperature and water vapor pressure were considered constant along the Peltier stage and in agreement with the measured values, although small differences may exist between actual and measured values.

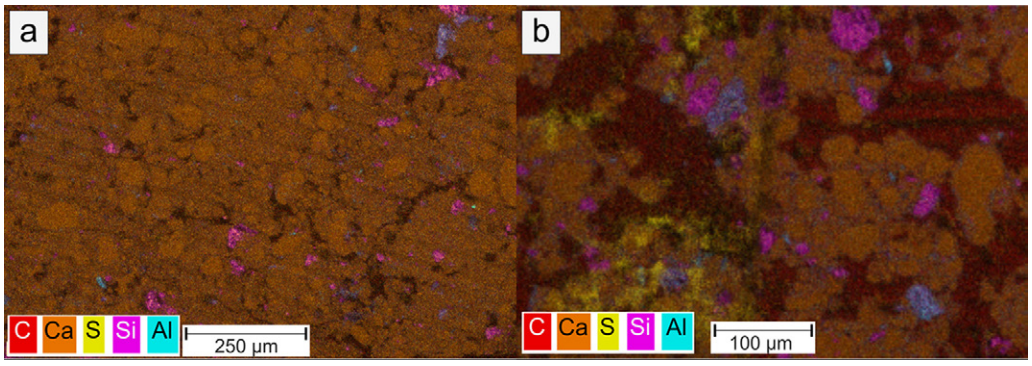

Fig. 3. General view of energy dispersive X-ray maps analysis for (a) the initial and (b) the 3-yr-irrigated sample.

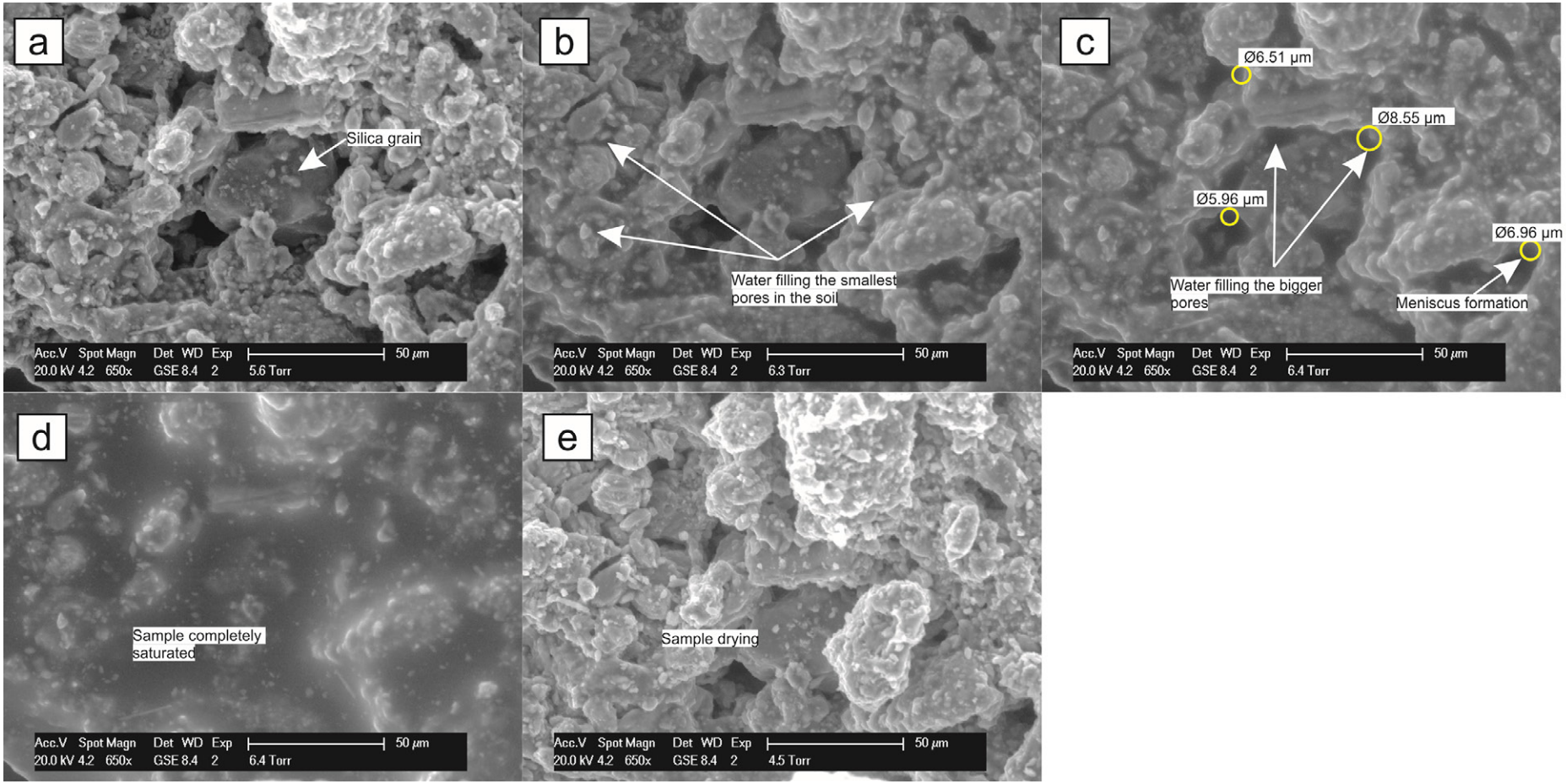

Fig. 4. Environmental scanning electron micrographs of initial soil sample pre-irrigation and detail of a silica particle and menisci during (a–d) wetting and (d–e) drying cycles.

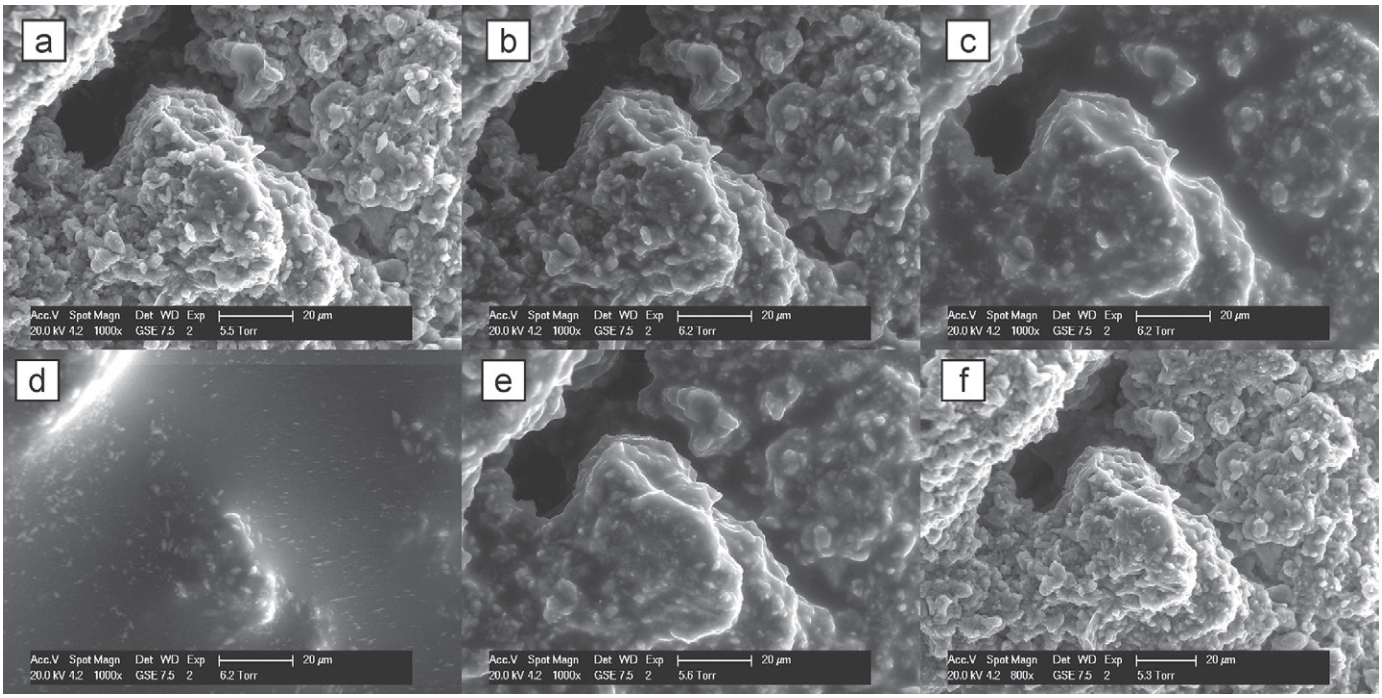

Fig. 5. Environmental scanning electron micrographs of a soil sample post-irrigation during (a–d) wetting and (d–f) drying cycles.

Analysis of the pre-irrigation sample establishes a reference stage to compare with results from the post-irrigation stage. It is difficult to obtain quantitative results from just the application of the dynamic mode analysis because no datasets exist to compare with. More dynamic ESEM analyses applied to different soil types are required to achieve conclusive results from the analysis of just one soil type.

Figure 5 displays the results of the wetting and drying process applied to the 3-yr-irrigated sample. The tubular calcite structures are dissolved after the wetting–drying cycle. Compared with the nonirrigated soil sample test, the wetting process takes place in a more continuous manner, starting with a lower water vapor pressure and with no sharp wetting steps. The RH at which complete sample saturation was achieved decreased from 98 to 100% for pre-irrigation samples to 86.4 to 95% (6.2–5.8 mm Hg) for post-irrigation samples. The irrigated sample presents high hydrophilic behavior, leading to generally higher soil water content due to the greater salt content of applied water. The evolution of a water droplet in the 3-yr-irrigated sample is shown in Fig. 6. The droplet remained unblended with soil water during the two first consecutive wetting–drying cycles, and during the third cycle it mixed with the surrounding water and eventually disappeared. Differences in salinity and viscosity between the droplet and the surrounding water have been described (Kwak et al., 2005; Lins and Azaiez, 2018).

No important differences between the three consecutive wetting–drying cycles were observed. The wetting–drying path was not exactly the same (i.e., the same pores were not filled in the same order); nevertheless, the vapor pressure value at which complete saturation was achieved remained almost constant (±0.1 mm Hg) for all three saturation times.

Discussion

Differences in the behavior of irrigated and nonirrigated soil samples are observed after the absence or presence of salt in the system. Full saturation is achieved at lower water vapor pressure in the post-irrigation sample in a similar way to how different saturation water vapor pressures are obtained in closed systems with different saturated salt solutions (ASTM, 1991; Herington, 1977). From this, it is expected that the soils had higher soil water contents; nevertheless, higher plant water availability cannot be concluded from the former effect because the increase in soil water content is counterbalanced by the soil pressure head decrease produced by the higher salt content in soil water. Irrigation with brackish water over a long period increases salt content in the soil–water system, and the equilibrium between liquid and vapor phases will evolve to a more thermodynamically stable liquid phase, explaining the observed experimental behavior.

The pre-irrigation sample wetting indicates a fast saturation and a continuous process for the post-irrigation sample. Changes in soil water composition may lead to condensation of very small amounts of water on the soil sample, as seen in Fig. 5e, where the sample surface is covered by a thin and homogeneous layer of water. Furthermore, water-borne salts may become part of the soil minerals as a consequence of the dissolution–precipitation process.

The salinity increase in soil water also explains the presence of unblended small droplets of soil water during the wetting–drying cycles. The salinity difference between deionized water in the vapor chamber and water in the soil would explain this process. Long-term irrigation with brackish water could lead to accumulation of salts, and in Valdes-Abellan et al. (2017) gypsum was identified as the main mineral to precipitate in the soil. The

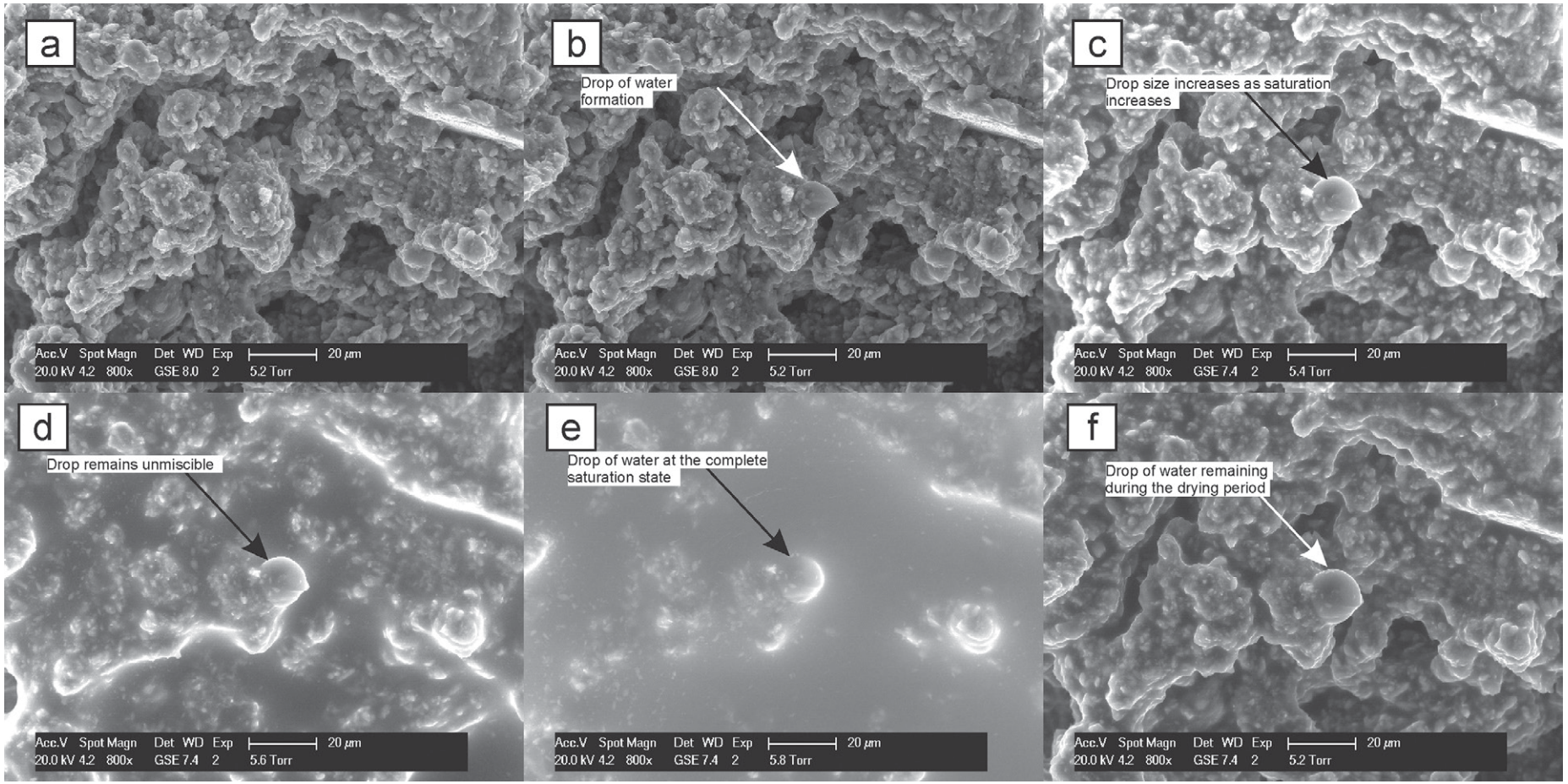

Fig. 6. Environmental scanning electron micrographs of a 3-yr-irrigated soil sample with a detail of a water droplet evolution: (a–e) wetting process; and (e–f) drying process.

impact on soil hydrophilic behavior depends on the type of salts present in the system, which depends on the soil mineralogy and the chemistry of the applied irrigation water. Therefore, a different impact on soil hydrophilicity can be expected under different environmental conditions.

The presence of a thermal gradient inside the analyzed samples was not considered based on the size and shape of the samples (i.e., roughly lenticular). The uniform condensation of water vapor in samples, as observed in the different images, supports our initial assumption. Nevertheless, important variations in temperature among different parts of the sample could lead to different behaviors along the sample soil surface.

The presence of heavy metals in the irrigated sample may be explained by the reverse osmosis desalination process. During the desalination process, water is conveyed through metal pipes, and the oxidation process could explain the presence of metals in the water applied and in the soil samples. Research by Abdul-Wahab and Jupp (2009), Akhand et al. (2011), and Mohamed et al. (2005) in the Middle East has also detected heavy metals in the water and in the vicinity of the brine outlet.

The ESEM technique not only reveals the hydrophilic–hydrophobic of patterns in soils; it may be used in many other applications (e.g., pore clogging and porous media scaling by mineral precipitation). The main disadvantages of the technique are related, from the authors' point of view, to the small sample size required by ESEM equipment. The small sample size may cause doubts about the representativeness of the results and their extrapolation to the complete soil layer. This is not a feature particular to the ESEM technique; it is extended to many other soil characterization procedures. Nevertheless, ESEM results should be considered carefully when conditions of nonuniformity are expected within the study area.

Conclusions

The results obtained from the ESEM technique of water application to the soil samples indicate (i) a change of soil hydrophilic behavior by the irrigation water–borne salt into the porous medium, (ii) a more gradual wetting process for the irrigated sample, (iii) a lower water vapor pressure value to start the wetting process in the irrigated sample, (iv) a lower water vapor pressure after sample saturation for the 3-yr-irrigated sample, and (v) the presence of heavy metals in soil produced by the reverse osmosis process.

Microscale observation of the drying–wetting cycle helps to explain the upscaling or modeling processes. Observed changes in hydrophilic behavior could be expected in similar vadose zone soils irrigated with nonfresh water.

The application of ESEM, in both static and dynamic modes, is a promising technique to study soil impacts from a new perspective. Further analysis is required to increase the number of results, which would let researchers build soil porous media diagnoses from ESEM results.

Acknowledgments

This study forms part of the CGL2013-48802-C3-3-R projects financed by the Spanish Ministry of Science and Innovation and of the GRE15-19 project financed by the University of Alicante (Spain).

References

Abdul-Wahab, S.A., and B.P. Jupp. 2009. Levels of heavy metals in subtidal sediments in the vicinity of thermal power/desalination plants: A case study. Desalination 244:261–282. doi:10.1016/j.desal.2008.06.007

Akhand, N.A., M.M. Al Mulla, F.K. Taha, Y.S. Hedar, and B.A. AlAraj. 2011. Evaluation of existing disposal practices of brine from the reverse osmosis desalination plants used for agriculture. Presented at: ASABE Annual International Meeting 2011, Louisville, KY. 7–10 Aug. 2011.

Ali, L., and M.A. Barrufet. 1995. Study of pore structure modification using environmental scanning electron microscopy. J. Pet. Sci. Eng. 12:323–338. doi:10.1016/0920-4105(94)00050-E

Allen, R.G., L.S. Pereira, D. Raes, and S. Martin. 1998. Crop evapotranspiration: Guidelines for computing crop water requirements. Irrig. Drain. Pap. 56. FAO, Rome.

Andraski, B.J., and B.R. Scanlon. 2002. Thermocouple psychrometry. In: J.H. Dane and G.C. Topp, editors, Methods of soil analysis. Part 4. Physical methods. SSSA Soil Ser. 5. SSSA, Madison, WI. p. 609–642. doi:10.2136/sssabookser5.4.c22

Assouline, S., and K. Narkis. 2011. Effects of long-term irrigation with treated wastewater on the hydraulic properties of a clayey soil. Water Resour. Res. 47:W08530. doi:10.1029/2011WR010498

Assouline, S., and K. Narkis. 2013. Effect of long-term irrigation with treated wastewater on the root zone environment. Vadose Zone J. 12(2). doi:10.2136/vzj2012.0216

ASTM. 1991. Standard E104-85: Standard practice for maintaining constant relative humidity by means of aqueous solutions. Vol. 11.07. Air quality. ASTM, West Conshohocken, PA.

Beltrán, J.M. 1999. Irrigation with saline water: Benefits and environmental impact. Agric. Water Manage. 40:183–194. doi:10.1016/S0378-3774(98)00120-6

Buckman, J. 2014. Use of automated image acquisition and stitching in scanning electron microscopy: Imaging of large scale areas of materials at high resolution. Microsc. Anal. 28:S13–S15.

Dikinya, O., C. Hinz, and G. Aylmore. 2008. Decrease in hydraulic conductivity and particle release associated with self-filtration in saturated soil columns. Geoderma 146:192–200. doi:10.1016/j.geoderma.2008.05.014

Donald, A.M. 1998. Environmental scanning electron microscopy for the study of 'wet' systems. Curr. Opin. Colloid Interface Sci. 3:143–147. doi:10.1016/S1359-0294(98)80006-X

Farulla, C.A., A. Ferrari, and E. Romero. 2010. Volume change behaviour of a compacted scaly clay during cyclic suction changes. Can. Geotech. J. 47:688–703. doi:10.1139/T09-138

Flint, A.L., and L.E. Flint. 2002a. Particle density. In: J.H. Dane and G.C. Topp, editors, Methods of soil analysis. Part 4. Physical methods. SSSA Book Ser. 5. SSSA, Madison, WI. p. 229–240. doi:10.2136/sssabookser5.4.c10

Flint, A.L., and L.E. Flint. 2002b. Porosity. In: J.H. Dane and G.C. Topp, editors, Methods of soil analysis. Part 4. Physical methods. SSSA Book Ser. 5. SSSA, Madison, WI. p. 241–253. doi:10.2136/sssabookser5.4.c11

Forster, A.M., G.M. Medero, T. Morton, and J. Buckman. 2008. Traditional cob wall: Response to flooding. Struct. Surv. 26:302–321. doi:10.1108/02630800810906557

Gee, G.W., and D. Or. 2002. Particle-size analysis. In: J.H. Dane and G.C. Topp, editors, Methods of soil analysis. Part 4. Physical methods. SSSA Book Ser. 5. SSSA, Madison, WI. p. 255–293. doi:10.2136/sssabookser5.4.c12

Ghermandi, A., and R. Messalem. 2009. The advantages of NF desalination of brackish water for sustainable irrigation: The case of the arava valley in Israel. Desalination Water Treat. 10:101–107. doi:10.5004/dwt.2009.824

Grossman, R.B., and T.G. Reinsch. 2002. Bulk density and linear extensibil-

ity. In: J.C. Dane and G.C. Topp, editors, Methods of soil analysis. Part 4. Physical methods. SSSA Book Ser. 5. SSSA, Madison, WI. p. 201–228. doi:10.2136/sssabookser5.4.c9

Herington, E. 1977. Recommended reference materials for realization of physicochemical properties. Pergamon Press, Oxford, UK.

Koliji, A., L. Vulliet, and L. Laloui. 2010. Structural characterization of unsaturated aggregated soil. Can. Geotech. J. 47:297–311. doi:10.1139/T09-089

Kwak, H.T., G. Zhang, and S. Chen. 2005. The effects of salt type and salinity on formation water viscosity and NMR responses. Presented at: International Symposium of the Society of Core Analysts, Toronto. 21–25 Aug. 2005.

Lado, M., and M. Ben-Hur. 2009. Treated domestic sewage irrigation effects on soil hydraulic properties in arid and semiarid zones: A review. Soil Tillage Res. 106:152–163. doi:10.1016/j.still.2009.04.011

Lado, M., and M. Ben-Hur. 2010. Effects of irrigation with different effluents on saturated hydraulic conductivity of arid and semiarid soils. Soil Sci. Soc. Am. J. 74:23–32. doi:10.2136/sssaj2009.0114

Lins, T.F., and J. Azaiez. 2018. Dynamic control of droplets and pockets formation in homogeneous porous media immiscible displacements. Phys. Fluids 30:032105.

Lourenço, S.D.N., D. Gallipoli, C.E. Augarde, D.G. Toll, P.C. Fisher, and A. Congreve. 2012. Formation and evolution of water menisci in unsaturated granular media. Geotechnique 62:193–199. doi:10.1680/geot.11.P.034

Lourenço, S.D.N., D.G. Toll, C.E. Augarde, D. Gallipoli, A. Congreve, T. Smart, et al. 2008. Observations of unsaturated soils by environmental scanning electron microscopy in dynamic mode. In: Unsaturated soils: Advances in geo-engineering. Proceedings of the 1st European Conference on Unsaturated Soils, Durham, UK. 2–4 July 2008. CRC Press, Boca Raton, FL.

Mandal, U.K., A.K. Bhardwaj, D.N. Warrington, D. Goldstein, A. Bar Tal, and G.J. Levy. 2008. Changes in soil hydraulic conductivity, runoff, and soil loss due to irrigation with different types of saline–sodic water. Geoderma 144:509–516. doi:10.1016/j.geoderma.2008.01.005

Martínez Beltrán, J., and S. Koo-Oshima. 2004. Water desalination for agricultural applications. In: Proceedings of the FAO Expert Consultation on Water Desalination for Agricultural Applications, Rome. 26–27 Apr. 2004. FAO, Rome.

Mohamed, A.M.O., M. Maraqa, and J. Al Handhaly. 2005. Impact of land disposal of reject brine from desalination plants on soil and groundwater. Desalination 182:411–433. doi:10.1016/j.desal.2005.02.035

Prats, D., and M.F. Chillón Arias. 2001. A reverse osmosis potable water plant at Alicante University: First years of operation. Desalination 137:91–102. doi:10.1016/S0011-9164(01)00207-7

Prats, D., M.F. Chillón, M. Rubio, and J.A. Reverte. 1997. Alicante University, closed water cycle, reverse osmosis and water treatment plants. Desalination 109:315–321. doi:10.1016/S0011-9164(97)00077-5

Romero, E., and P.H. Simms. 2008. Microstructure investigation in unsaturated soils: A review with special attention to contribution of mercury intrusion porosimetry and environmental scanning electron microscopy. Geotech. Geol. Eng. 26:705–727. doi:10.1007/s10706-008-9204-5

Dane, J.H., and G.C. Topp, editors. 2002. Methods of soil analysis. Part 4. Physical methods. SSSA Book Ser. 5. SSSA, Madison, WI. doi:10.2136/sssabookser5.4

Valdes-Abellan, J., L. Candela, J. Jiménez-Martínez, and J.M. Saval-Pérez. 2013. Brackish groundwater desalination by reverse osmosis in southeastern Spain. Presence of emerging contaminants and potential impacts on soil-aquifer media. Desalination Water Treat. 51:2431–2444. doi:10.1080/19443994.2012.747506

Valdes-Abellan, J., J. Jiménez-Martínez, and L. Candela. 2014. Dispersivity determination through a modeling approach from a tracer test based on total Br concentration in soil samples. Soil Sci. 179:403–408.

Valdes-Abellan, J., J. Jiménez-Martínez, L. Candela, D. Jacques, C. Kohfahl, and K. Tamoh. 2017. Reactive transport modelling to infer changes in soil hydraulic properties induced by non-conventional water irrigation. J. Hydrol. 549:114–124. doi:10.1016/j.jhydrol.2017.03.061

Valdes-Abellan, J., J. Jiménez-Martínez, L. Candela, and K. Tamoh. 2015. Comparison among monitoring strategies to assess water flow dynamic and soil hydraulic properties in agricultural soils. Span. J. Agric. Res. 13(1):e1201. doi:10.5424/sjar/2015131-6323